Hydrolysis-induced immobilization of $Pt(acac)_2$ on polyimide-based carbon nanofiber mat and formation of Pt nanoparticles†

Nguyen Thi Xuyen,[a] Hae Kyung Jeong,[b] Gunn Kim,[b] Kang Pyo So,[a] Kay Hyeok An[c] and Young Hee Lee*[ab]

Received 4th August 2008, Accepted 2nd December 2008
First published as an Advance Article on the web 26th January 2009
DOI: 10.1039/b813486c

Electrospun polyimide (PI)-based carbon nanofibers have recently garnered much interest due to their high conductivity and high mechanical strength. Promising applications include electrodes for supercapacitors, filters, sensors, and fuel cells. Here, we demonstrate that Pt nanoparticles can be loaded on the surface of PI nanofibers *via* an immobilization process induced by hydrolysis. The uniform distribution and sizes of Pt nanoparticles were controlled further by carbonization. $Pt(acac)_2$ dissolved in acetone was impregnated on the hydrolyzed PI nanofibers. Pt ions were localized exclusively on the surface of PI nanofibers by precise control of the hydrolysis process. Our X-ray photoelectron spectroscopy results show that Pt ions in $Pt(acac)_2$ molecules (40%) are immobilized on the hydrolyzed PI surface while some of them (60%) bind to O in the carboxylic group to form a PtO structure, and then are fully decomposed into Pt nanoparticles during carbonization. Using density functional calculations, we show that the binding of $Pt(acac)_2$ on hydrolyzed PI is strong with a binding energy of −4.3 eV, which originates mostly from Pt–O binding and π-stacking between (acac) and PAA, confirming experimental observations of robust formation of Pt nanoparticles on hydrolyzed PI. The cyclic voltammetric test demonstrates that our robust carbon nanofiber mat can be utilized for fuel cell electrodes.

Introduction

Nanoparticles (NPs) are interesting for materials science because of their unique electronic, optical, magnetic, catalytic properties and their multifunctional capabilities for diverse applications.[1–6] In the application for fuel cells, NPs need to be loaded on the supporting materials. The supporting material should be conductive and highly permeable. They are in general carbon-based, *i.e.*, activated carbons,[7–9] carbon nanotubes,[3,4,10] and carbon nanofibers.[11–14] However, most of these supports are a powder type that requires the use of an additional binder to form a sheet-type electrode, where the binder is a source of the degradation of electrical conductivity.[11] To synthesize Pt NPs on the support, one uses some physical methods such as sputtering, evaporation (commercial product Etek), and numerous chemical methods which are cheap and scalable for mass production. In the latter, controlling the nanometer size and uniform distribution of Pt NPs without agglomeration and high loading amount simultaneously is still a challenging issue for the general purpose of catalysts. Three types of metallic precursors exist: (i) metal salts (for instance, Pt, $PtCl_2$, $PtCl_4$), (ii) metal complexes such as platinum acetylacetonate, $Pt(acac)_2$,[15] and platinum o-benzoquinonediimine, $Pt(bqdi)_2$,[16] dissolved in an organic solvent, and (iii) metal complexes dissolved in water (K_2PtCl_6, H_2PtCl_6).[3,4] These materials can be impregnated into supports and a reduction agent is necessarily used to control the particle size. Because the metal salts are ionized in water and are not easily absorbed onto the organic support surface, it is impossible to obtain high loading amounts of metal ions on carbon-based supports.[10–14] In addition, maintaining particle sizes at less than 3 nm with a monodisperse size distribution seems to be rather difficult due to unstable anchoring of metal ions on the support during the reduction process. As a result, organometallic aromatic compounds such as $Pt(acac)_2$ have been recently used to overcome this difficulty.[15,17–19] The organometallic aromatic compounds are designed to be easily soluble in an organic solvent. In general, organometallic aromatic compounds adsorb on the support first and are believed to be decomposed into metal ions during thermal annealing, which is different from the reduction process in the case of a metal salt. It has been reported that the immobilization of $Pt(acac)_2$ under supercritical conditions leads to embedded nanoparticles in the polyimide film.[15] $Fe(acac)_3$, $Pt(acac)_2$, and $Cu(acac)_2$ can be immobilized on silicon substrate in different ways.[20,21] However, the mechanism during adsorption has yet to be clearly explained. One important feature to note is that the immobilization strength also depends on the shape of the complex, the surface functional groups, and the choice of the support. Another advantage of using organometallic aromatic compounds is that an aggregation of metal ions is limited by the presence of organic compounds even under high temperature annealing.

[a]*Sungkyunkwan Advanced Institute of Nanotechnology, Center for Nanotubes and Nanostructured Composites, Sungkyunkwan University, Suwon, 440-746, Korea. Fax: +82 31 290 5954; Tel: +82 31 299 6507*
[b]*Department of Physics, Sungkyunkwan University, Suwon, 440-746, Korea. Fax: +82 31 290 5954; Tel: +82 31 299 6507*
[c]*Material & Development Department, Jeonju Machinery Research Center, Jeonju, 561-844, Korea. Fax: + 82 63 214 3561; Tel: + 82 63 214 3504*

† Electronic supplementary information (ESI) available: SEM images of PI hydrolyzed nanofibers; molecule structures of $Pt(acac)_2$, PAA and PI; models of absorption of $Pt(acac)_2$ molecule on PAA and PI; table of absorption energies, closest separation distances between $Pt(acac)_2$ and PAA/PI, and amount of charge transfer from $Pt(acac)_2$ to PAA or PI. See DOI: 10.1039/b813486c

PI nanofiber mats are well known to be carbonized to carbon nanofiber mats under high temperature annealing, which serve as excellent electrodes for supercapacitors.[22–24] A self-assembled nanofiber mat can, in principle, achieve relatively high electrical conductivity by a binder-free process and a large surface area is attainable due to the formation of small-diameter nanofibers in the mat.[25] Furthermore, PI films can be hydrolyzed by KOH to be transformed to poly(amic acid) (PAA) which can be subsequently used to incorporate versatile metallic ions.[26–30] The processes of these studies have been combined to produce metal NP/PI composites by using hydrogen gas reduction at less than 400 °C. However, these approaches have not met the requirements for fuel cell applications yet.

The purpose of this paper is threefold: (i) to understand the underlying mechanism of immobilization of metal organic compounds on the support, (ii) to locate Pt nanoparticles near the support surface, and (iii) to form the nanoparticles uniformly over the support surface with high density. The location of Pt ions was achieved by mild hydrolysis of electrospun PI nanofibers followed by a droplet of $Pt(acac)_2$ solution. Firing PI nanofibers in Ar gas was conducted to form uniform-sized particles on the nanofiber surface and carbonize PI into carbon. The underlying mechanism was analyzed by X-ray photoelectron spectroscopy (XPS) and density functional calculations. Lastly, the current behaviour of Pt-loaded carbon nanofibers in cyclic voltammetry tests indicates favorable catalytic properties for fuel cell applications.

Experimental

Support preparation

Polyimide (PI) nanofiber mats were prepared as a supporting precursor matrix for nucleating Pt nanoparticles. The nanofiber mats were synthesized by electrospinning a poly(amic acid) (PAA) solution with high molecular weight dissolved in *N*,*N*-dimethylformamide (Sigma Aldrich, 99.8%). The PI nanofiber mats were then obtained by stabilizing the PAA nanofiber mats described in a previous work.[25] After being washed with isopropanol and deionized water for 3 minutes the PI nanofiber mats were dried in an oven to remove any residual solvent. The PI nanofiber mats were immersed into a KOH solution of 0.1 M for hydrolysis at room temperature for 2 minutes. The hydrolyzed PI nanofibers were neutralized using a 0.5 M HCl solution for 5 minutes at room temperature and then washed again with deionized water and isopropanol. To prevent the functional shells of the polyimide nanofibers from being inverted into polyimide, the hydrolyzed PI nanofibers were dried under vacuum at room temperature and used to perform Pt nucleation immediately.

Pt nucleation

$Pt(acac)_2$ (Sigma Aldrich, 97%) was dissolved in acetone. This solution was dropped onto hydrolyzed PI nanofiber mats to nucleate Pt ions coordinated with the carboxylic acid groups on the surface of PI nanofibers. The amount of Pt loaded was fixed at 10% of the PI weight. The Pt-loaded PI nanofiber mats were put between two ceramic plates and fired to 900 °C in Ar gas with different heating rates and kept at 900 °C for 30 minutes. The experimental procedures of each step are shown in Fig. 1.

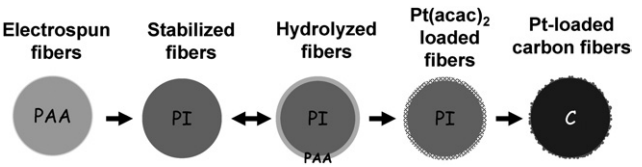

Fig. 1 The scheme for the loading of Pt nanoparticles on PI-based carbon nanofibers.

Measurements

For transmission electron microscope (TEM) measurements, the prepared Pt-loaded PI nanofiber mats were ground into small fragments. This powder was dissolved in ethanol and sonicated in a bath-type sonicator (Power Sonic 505, Hwashin) for a minute or less to get individually dispersed nanofibers. This solution was then dropped onto a carbon TEM grid and dried in a vacuum furnace. TEM images were taken using a field emission JEM 2010F, JEOL at 200 kV. The selected area electron diffraction patterns and the corresponding Fourier transformed patterns were taken during TEM observations. The Pt-loaded nanofiber mats were directly used for X-ray diffraction (XRD) with a Cu anode (1.54 Å) using a D8 DISCOVER - BRUKER AXS. Pearson and Scherrer equations were used to fit the curve and calculate the particle size at different Pt peaks [111], [200], [220]. The interaction between $Pt(acac)_2$ and the poly(amic acid) surface was investigated by X-ray photoelectron spectroscopy (XPS). $Pt(acac)_2$ in acetone was dropped onto an Au/Si substrate which was covered with Ag paste at the edges. A hydrolyzed PI mat was prepared by immersing it in $Pt(acac)_2$/acetone and subsequently washing it with acetone to remove any excess $Pt(acac)_2$. Scanning electron microscopy (SEM, JEOL JSM6700F) was used to observed the morphology of the carbon nanofibers. Thermogravimetric analysis (TGA) was used to measure the amount of Pt in the carbon nanofiber mats. The cyclic voltammetry was performed using a Solatron 1400 series three electrode system. The samples were ground and dispersed in isopropanol by sonication and then a certain amount was dropped onto the graphite electrode. The test was done in methanol 0.5M/H_2SO_4 0.25 M at a scanning rate of 50 mV/s. The methanol/H_2SO_4 solution was bubbled with N_2 gas for 30 min to remove molecular oxygen right before the CV measurements. E-tek samples of 20% Pt on Vulcan XC-72 (lot #JJ121506) were used as reference electrodes. The data shown in Fig. 5a are from the 33rd scanning cycle.

Computational details

We carried out first-principles pseudopotential calculations within local density approximations using a linear combination of atomic orbitals (LCAO) basis set, implemented with the $DMol_3$ package. The double numerical quality basis set, with a polarization d-function (DND), is employed in which 2s, 2p and 3d orbitals for carbon, oxygen, and nitrogen respectively, 4f, 5d, 6s and 6p orbitals for platinum, and 1s for hydrogen are included. We used norm-conserving DFT semicore pseudopotentials

(DSPP) to describe the interaction between the core and valance electrons. Real space orbital cutoffs were 3.0 Å for hydrogen, carbon, oxygen, nitrogen, and 3.4 Å for platinum. The supercell is $20 \times 10 \times 8$ Å^3. Our model structures were fully optimized until the Hellman–Feynman forces were reduced to within 0.04 Ha Å^{-1} (Ha = hartree, 1 Ha = 2 Rydberg = 27.2 eV). The adsorption energy of $Pt(acac)_2$ is calculated as the difference of total energies between an adsorbed system and the separate species, $E_b[Pt(acac)_2] = E[Pt(acac)_2 + polymer] - E(polymer) - E[Pt(acac)_2]$.

Results and discussion

The issue here is how to *locate* Pt atoms near the surface layer of PI nanofibers. The PI film has been hydrolyzed under strong conditions to be converted to PAA.[26–30] The main effect of hydrolysis is to transform PI to PAA by breaking aromatic rings and to further etch away PAA layers.[31] However, these conditions were too severe to locate Pt ions near the surface. For the case of PI nanofibers, the etching effect was dominant at high KOH concentrations due to small diameters so that the nanofibers were melted (see ESI† Fig. S1). The hydrolysis conditions of KOH concentration, treatment time, and temperature are all important factors in determining the thickness of PAA layers (or hydrolyzed PI layers).[32] A PAA layer thickness of less than 10 nm is desired to locate Pt nanoparticles on the surface after carbonization. With short treatment times and mild KOH concentrations at room temperature, described in the Experimental section, the morphology of the carbonized nanofiber mats was not altered (Fig. 2a). Furthermore Pt nanoparticles were localized on the fiber surface. The morphology of the robust porous mats was preserved by the mild hydrolysis conditions and simultaneously keeping the supporter at the static state during carbonization. The conductivity of the Pt-loaded CNF mats was also not altered (15 S cm^{-1}).

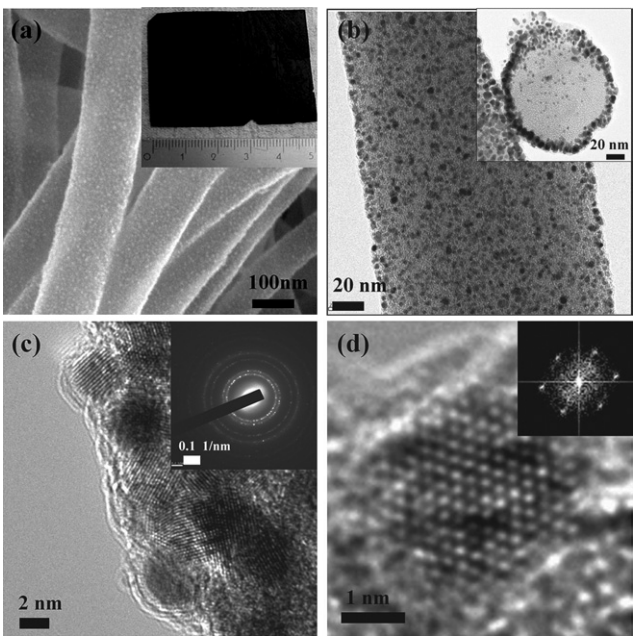

Fig. 2 (a) SEM image of a Pt-loaded carbon nanofiber mat. The inset is its optical micrograph. (b) TEM image of a Pt-loaded carbon nanofiber and its cross section (inset). (c) High resolution TEM image and SAED (inset), and (d) higher resolution TEM image of a single Pt nanoparticle showing the fcc structure with its FFT electron diffraction in the inset.

The overall process for NP formation is suggested as follows. Thin surface layers of PI nanofibers, without altering the inner cores, were transformed into PAA during hydrolysis. The PAA layers are hydrophilic with carboxyl groups. This enables $Pt(acac)_2$ to adsorb easily onto the PAA surface or to penetrate into the PAA layers in the form of Pt oxide. During the carbonization process, two different reaction steps are involved. The first step is to transform PAA to PI nanofibers.[29] The second step is to form Pt nanoparticles. The bare Pt atoms are released from the PI network and from the (acac) ligand. (Acac) may be easily decomposed under heat treatment thus freeing the Pt atom.[20] These Pt atoms migrate to form Pt clusters during high temperature annealing. Under the conditions of carbonization at 900 °C, Pt nanoparticles were uniformly distributed over the nanofibers (Fig. 2b). The size and distribution of particles strongly rely on the carbonization conditions, which will be discussed later. The cross section of the carbonized nanofiber in the inset of Fig. 2b clearly illustrates that Pt nanoparticles were located near the surface of the carbonized nanofiber with a thickness of less than 10 nm.[33] The selected area electron diffraction pattern in Fig. 2c shows discrete spots (inset), which is evidence theat each Pt nanoparticle grows in different orientations. The Pt nanoparticles obtained were highly crystalline due to the annealing at high temperature (Fig. 2d). It is worth noting that without the hydrolysis process, Pt nanoparticles were rarely loaded on the carbon nanofibers.

XPS was performed for Pt and C elements in order to understand the underlying mechanism of Pt adsorption. Fig. 3a shows XPS spectra of Pt4f from $Pt(acac)_2$ powder, and $Pt(acac)_2$-loaded PAA surface before carbonization. From the spectrum of $Pt(acac)_2$, $Pt(acac)_2$ was identified by four main peaks (Fig. 3b). The binding energies of $Pt(acac)_2$ powder are listed in Table 1. Two groups of peaks (1, 3) and (2, 4) were related to different oxidation states. Two peaks in (1, 3) or (2, 4) differentiated by about 3 eV correspond to two respective spin states of $Pt4f_{5/2}$ and $Pt4f_{7/2}$.[34] The binding energies of PtO, PtO_{ads}/$PtOH_{ads}$ and PtO_2 obtained from platinum oxides are listed in Table 1 from references 35 and 36. It is noted that the peak positions of our $Pt(acac)_2$ powder were slightly different from those of platinum oxides. These peaks come from bonds between Pt and O in $Pt(acac)_2$ ligands. Another source of Pt–O interaction is Pt ions with oxygen atoms in the adjacent $Pt(acac)_2$ due to unsaturated axial ligands of Pt ions.[16] The analysis of $Pt(acac)_2$-loaded PAA is based on the above assignment of $Pt(acac)_2$. In order to analyze the spectra of $Pt(acac)_2$-loaded PAA, the known values of binding energies and the ratio of the integrated area among peaks of $Pt(acac)_2$ were used in the deconvolution while the values for the other species related to Pt were determined from the best fit. Their binding energies are listed in Table 1. In addition to $Pt(acac)_2$ peaks, four new peaks were observed in $Pt(acac)_2$-loaded PAA. These were identified to originate from $Pt(acac)_2$ adsorbed on O and/or OH functional groups (dashed line) of PAA and new PtO bonds (dotted line) formed between $Pt(acac)_2$ and PAA[35,36] (Fig. 3c). The relative compositions of the new PtO-related bonds and pristine $Pt(acac)_2$ were 60% and 40%, respectively. Moreover, the C1s spectrum in Fig. 3d also showed

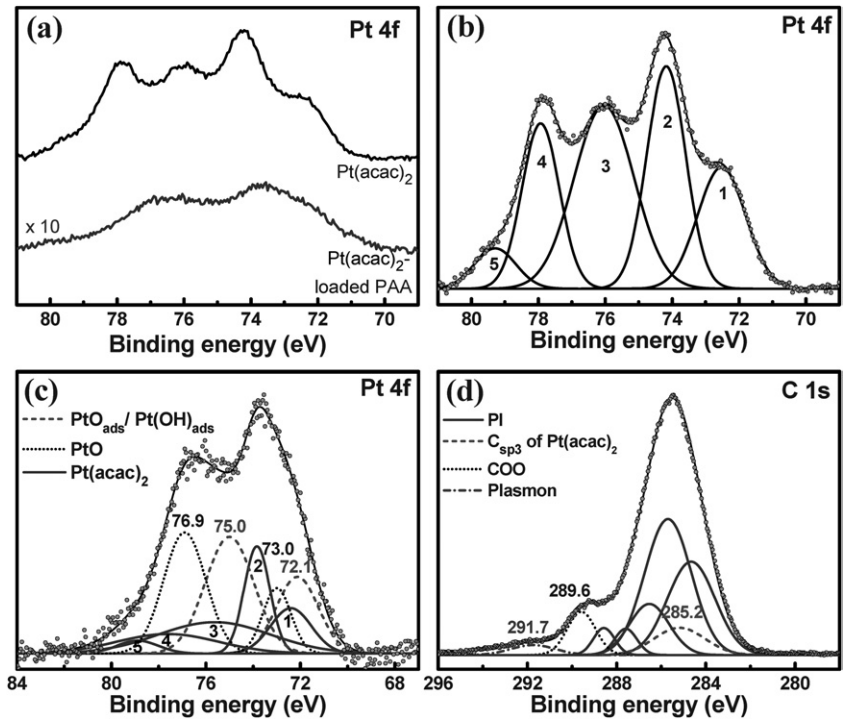

Fig. 3 XPS spectra of (a) Pt4f of $Pt(acac)_2$ and $Pt(acac)_2$-PAA nanofibers. Deconvoluted curves of (b) $Pt(acac)_2$ and (c) $Pt(acac)_2$-PAA nanofibers. (d) XPS spectra of C1s of $Pt(acac)_2$-PAA nanofibers.

Table 1 XPS data analysis of Pt4f including component peak positions and area ratio of $Pt(acac)_2$ and $Pt(acac)_2$-loaded PAA

Pt4f Binding energy/eV	$Pt(acac)_2$					PtO		PtO_{ads}/ $Pt(OH)_{ads}$		PtO_2	
	Peak 1	Peak 2	Peak 3	Peak 4	Peak 5	4f7/2	4f5/2	4f7/2	4f5/2	4f7/2	4f5/2
Reference 35,36 $Pt(acac)_2$ powder	72.5	74.2	76.0	77.9	79.3	73.3	76.3	72.1	75.0	73.9	77.2
$Pt(acac)_2$-loaded PAA	72.4	73.8	75.6 40%	77.6	78.9	73.0 26%	76.9	72.1 34%	75.0		

Table 2 The binding energy of C1s corresponding to functional groups of $Pt(acac)_2$-loaded PAA nanofibers

C1s	Csp^2(ODA)	Csp^2(PMDA) and C–N	C–OH	C–O–C	C═O	Csp^3 of $Pt(acac)_2$	COOH	Plasmon
Binding energy (eV)	284.7	285.7	286.5	287.6	288.6	285.2	289.6	291.7

sp^3 bonds near 285.2 eV (dotted line) which was caused by the interaction of PAA with (acac) ligands. Other PAA-related peaks are listed in Table 2.[37] More specifically, 40% of $Pt(acac)_2$ were simply adsorbed on the PAA surface, whereas 60% of $Pt(acac)_2$ were decomposed into Pt atoms to form PtO related bonds with PAA. It is understood that PtO bonds are chemically strong. However, it is not certain how $Pt(acac)_2$ molecules interact with PAA, let alone how strong they are.

To verify the nature of $Pt(acac)_2$ binding on PAA, we calculated the absorption energies for two different configurations, as shown in Fig. 4. The key parameters for adsorption are listed in Table S1 (ESI).† $Pt(acac)_2$ interacted with an oxygen atom in a carboxyl (–COOH) group in PAA, giving an adsorption energy of −3.58 eV (Fig. 4a). The adsorption was stronger when $Pt(acac)_2$ overlapped with PAA (Fig. 4b). In this case, Pt–O bonding was constructed and furthermore the binding was enhanced by the enhanced π-stacking interactions, resulting in an adsorption energy of −4.35 eV. No practical charge transfer was involved in either adsorption configuration. The latter adsorption configuration shows a high adsorption energy, which survives during carbonization at high temperature. These energetics provide several intuitive pictures of the nature of $Pt(acac)_2$ adsorption. The immobilization of $Pt(acac)_2$ on PAA is realized by both formation of PtO bonds invoking dipole interactions between two structures and π-stacking interactions which is ascribed to the planar nature of $Pt(acac)_2$. This immobilization

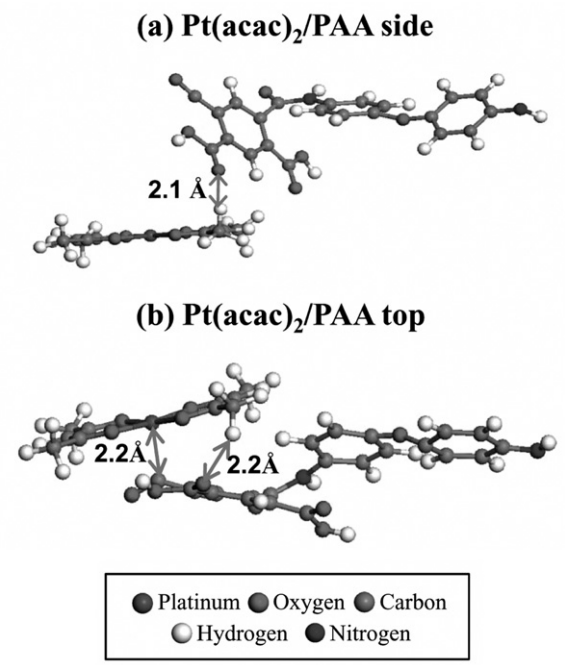

Fig. 4 Models of the absorption $Pt(acac)_2$ molecule on (a) PAA side and (b) PAA top.

leads to high loading amount of Pt nanoparticles that was experimentally corroborated in our work. This is in good contrast with three-dimensional $Fe(acac)_3$, where the immobilization of this material on silicon substrate has not been realized easily.[20,21]

CV characteristics were measured to investigate the activity of Pt nanoparticles in methanol oxidation, as shown in Fig. 5a. An E-tek sample with Pt loading amount of 20% of the weight was used as a comparison. We used the carbon nanofiber sample with a Pt loading amount equal to 20% of the weight. The currents were normalized with respect to the sample area and Pt loading amount. The forward anodic peak around 0.65 V vs. Ag/AgCl KCl saturated was due to the oxidation of methanol, *i.e.*, release of electrons. The peak position is related to the existence of Schottky barriers formed by an accumulation of oxides on the electrode or the Pt nanoparticles.[38] The lower value (0.7 V) of the E-tek electrode is partially indicative of the efficiency of the Pt catalyst or the electrode. The oxidation current (I_f = 42.9 mA) was also higher than that (34.3 mA). During the reverse scan, the oxidation peak at 0.55 V was obtained with a peak current of I_b = 24.0 mA. This peak is attributed to the release of adsorbed CO or CO-like species, which can be generated *via* incomplete oxidation of methanol in the forward scan. Thus, I_b indicates an accumulation of CO-like species, whereas I_f indicates the degree of complete methanol oxidation. Therefore, the ratio I_f/I_b is a measure of the efficiency of the Pt catalyst and CO tolerance. The ratio was about 1.8 for our sample, larger than the ratio of 1.1 which was calculated for the E-tek sample. The high ratio is attributed to (i) the robust formation of the mat and the high conductivity of carbon nanofibers and (ii) the high catalyst loading amount of monodisperse Pt nanoparticles that are well distributed over the surface in our sample. Moreover, Pt/carbon nanofibers exhibit electrocatalytic cycling stability, as shown in Fig. 5b. The current density of methanol oxidation is stable up to 33 scanning cycles without an appreciable degradation in the current.

Conclusions

We have demonstrated how to immobilize $Pt(acac)_2$ on polyimide nanofiber surfaces *via* hydrolysis. High amounts of Pt loading with Pt particle sizes less than 3 nm were realized on hydrolyzed polyimide nanofibers. The XPS analyses combined with density functional calculations lead us to conclude that the immobilization of $Pt(acac)_2$ on PAA is realized by both the formation of PtO bonds of dipole interactions and π-stacking interactions with a relative composition of 60% and 40%, respectively. Our approach provides a simple and practical route to load Pt nanoparticles uniformly over the surface of carbon nanofibers, which can be utilized for future fuel cell applications.

Acknowledgements

This work was financially supported by STAR-faculty project from MOE and in part by the KOSEF through CNNC at SKKU, and MOE, MOCIE, and MOLAB through the foresting project of laboratory of excellence.

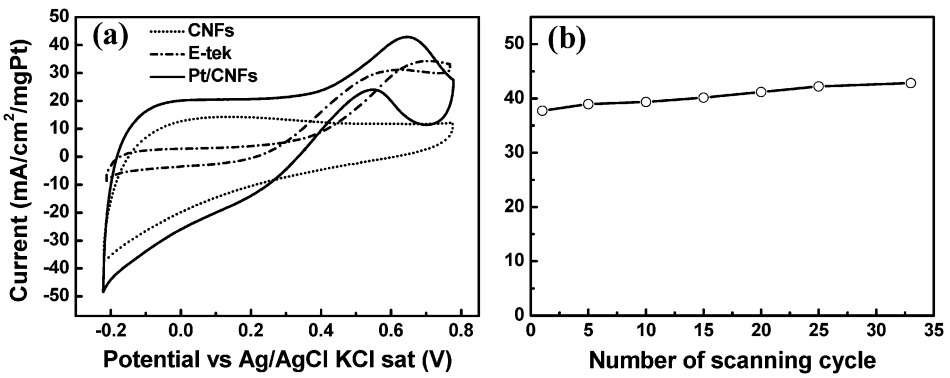

Fig. 5 (a) Cycle voltammetry of E-tek, Pt/carbon nanofibers, and carbon nanofiber mat without Pt loading, (b) electrocatalytic cycling stability of Pt/carbon nanofibers in 0.5 M methanol/0.25 M H_2SO_4 at a scanning rate of 50 mV/s.

References

1 G. Schmid, *Chem. Rev.*, 1992, **92**, 1709–1727.
2 G. A. Somorjai, A. M. Contreras, M. Montano and R. M. Rioux, *Proc. Natl. Acad. Sci. USA*, 2006, **103**, 10577–10583.
3 G. G. Wildgoose, C. E. Banks and R. G. Compton, *Small*, 2006, **2**, 182–193.
4 V. Georgakilas, D. Gournis, V. Tzitzios, L. Pasquato, D. M. Guldi and M. Prato, *J. Mater. Chem.*, 2007, **17**, 2679–2694.
5 V. L. Colvin and K. M. Kulinowski, *Proc. Natl. Acad. Sci. USA*, 2007, **104**, 8679–8680.
6 A. W. Cattleman Jr. and P. Jena, *Proc. Natl. Acad. Sci. USA*, 2006, **103**, 10554–10559.
7 J. Xi, J. Wang, L. Yu, X. Qiu and L. Chen, *Chem. Commun.*, 2007, 1656–1658.
8 R. Benítez, A. M. Chaparro and L. Daza, *J. Power Source*, 2005, **151**, 2–10.
9 S. H. Joo, S. J. Oh, I. Choi, J. Kwak, Z. Liu, O. Terasaki and R. Ryoo, *Nature*, 2001, **412**, 169–172.
10 B. Xue, P. Chen, Q. Hong, J. Lin and K. L. Tan, *J. Mater. Chem.*, 2001, **11**, 2378–2381.
11 Y. L. Hsin, K. C. Hwang and C. T. Yeh, *J. Am. Chem. Soc.*, 2007, **129**, 9999–10010.
12 E. S. Steigerwalt, G. A. Deluga and C. M. Lukehart, *J. Phys. Chem. B*, 2002, **106**, 760–766.
13 M. Endo, Y. A. Kim, M. Ezaka, K. Osada, T. Yanagisawa, T. Hayashi, M. Terrones and M. S. Dresselhaus, *Nano Lett.*, 2003, **3**, 723–726.
14 J. Guo, G. Sun, Q. Wang, G. Wang, Z. Zhou, S. Tang, L. Jiang, B. Zhou and Q. Xin, *Carbon*, 2006, **44**, 152–157.
15 S. Yoda, A. Hasegawa, H. Suda, Y. Uchimaru, K. Haraya, T. Tsuji and K. Otake, *Chem. Mater.*, 2004, **16**, 2363–2368.
16 J. C. Kenvin, M. G. White and M. B. Mitchell, *Langmuir*, 1991, **7**, 1198–1205.
17 H. Yano, M. Kataoka, H. Yamashita, H. Uchida and M. Watanabe, *Langmuir*, 2007, **23**, 6438–6445.
18 K. Matsuoka, K. Miyazaki, Y. Iriyama, K. Kikuchi, T. Abe and Z. Ogumi, *J. Phys. Chem. C.*, 2007, **111**, 3171–3174.
19 X. Teng, S. Maksimuk, F. S. rommer and H. Yang, *Chem. Mater.*, 2007, **19**, 36–41.
20 S. G. Fiddy, M. A. Newton, T. Campbell, A. J. Dent, I. Harvey, G. Salvini, S. Turin and J. Evans, *Phys. Chem. Chem. Phys.*, 2002, **4**, 827–834.
21 J. C. Kenvin, M. G. White and M. B. Mitchell, *Langmuir*, 1991, **7**, 1198–1205.
22 K. S. Yang, D. D. Edie, D. Y. Lim, Y. M. Kim and Y. O. Choi, *Carbon*, 2003, **41**, 2039–2046.
23 C. Kim, Y. O. Choi, W. J. Lee and K. S. Yang, *Electrochim. Acta*, 2004, **50**, 883–887.
24 C. W. Nah, S. H. Han, M. H. Lee, J. S. Kim and D. S. Lee, *Polym. Int.*, 2003, **52**, 429–432.
25 N. T. Xuyen, E. J. Ra, H.-Z. Geng, K. K. Kim, H. K. An and Y. H. Lee, *J. Phys. Chem. B*, 2007, **111**, 11350–11353.
26 K. Akamatsu, S. Ikeda, H. Nawafune and S. Deki, *Chem. Mater.*, 2003, **13**, 2488–2491.
27 T. H. Baum, D. C. Miller and T. R. OToole, *Chem. Mater.*, 1991, **3**, 714–720.
28 K. Akamatsu, H. Shinkai, S. Ikeda, S. Adachi, H. Nawafune and S. Tomita, *J. Am. Chem. Soc.*, 2005, **127**, 7980–7981.
29 S. Ikeda, K. Akamatsu, H. Nawafune, T. Nishino and S. Deki, *J. Phys. Chem. B*, 2004, **108**, 15599–15607.
30 Y. Li, Q. Lu, X. Qian, Z. Zhu and J. Yin, *Appl. Surf. Sci.*, 2004, **233**, 299–306.
31 L. J. Matienzo and W. N. Unertl, *Polyimides: Fundamental Aspects and Technological Applications*, Mittal K L, Ghosh, M Dekker, New York, 1996.
32 When the hydrolyzed sample was exposed to air for several days, large Pt particles were formed with a large separation distance between particles. The OH_- in the carboxyl group is not stable in air and can be easily detached. This causes a closure of aromatic rings to recover the PI structure. The number of active sites was reduced but instead the size of particles became larger. Therefore Pt loading has to be done immediately after hydrolysis (Fig. S2†).
33 Some Pt particles were removed during sample preparation for TEM observations and deposited into the inner cross sectional area. Those are visible in the TEM image.
34 J. Chastain and R. C. King, Jr., *Handbook of X-ray Photoelectron Spectrotroscopy*, Physical Electronics, Eden Prairie, MN, 1995.
35 K. S. Kim, N. Winograd and R. E. Davis, *J. Am. Chem. Soc.*, 1971, **93**, 6296–6297.
36 C. Huang, K. S. Tan, J. Lin and K. L. Tan, *Chem. Phys. Lett.*, 2003, **371**, 80–85.
37 D. Wolany, T. Fladung, L. Duda, J. W. Lee, T. Gantenfort, L. Wiedmann and A. Benninghoven, *Surf. Interface Anal.*, 1999, **27**, 609–617.
38 R. Mancharan and J. B. Goodenough, *J. Mater. Chem.*, 1992, **2**, 875–887.